

A POLYGONAL GENERALIZED FINITE ELEMENT FOR UNIDIRECTIONAL COMPOSITE MICROSTRUCTURE SIMULATION

Murilo Sartorato¹

¹ Sao Paulo State University, Campus Sao Joao da Boa Vista, School of Engineering (FESJ)
(murilo.sartorato@unesp.br)

Keywords: generalized finite elements, composite microstructure, polygonal finite elements, representative volume elements

ABSTRACT

Several works have been made on the simulation of unidirectional composite microstructure using Representative Volume Elements (RVE). These simulations, especially for the consideration of non-uniform distributed fibers tend to be computationally expensive, using hundreds of thousands of finite elements to complete. In the present work, a generalized finite element approach to the simulation of RVEs is shown. A polygonal generalized finite element enriched in such way that a circular fiber naturally exists in its domain is made to efficiently simulate a composite microstructure by using its Voronoi cells as a natural mesh. This proposition is not aimed at perfect accuracy comparing to traditional methods but to be a computationally efficient procedure for the simulation of non-uniform fiber unidirectional composite microstructures to use in either identifying critical regions through statistical analysis that need several realizations or to create synthetic populations for optimization or training artificial neural networks that study RVEs. Results of the approach for accuracy and computational time are shown and compared to a classical approach using the ABAQUS commercial finite element software. Accuracy of up to 98% were obtained for maximum stress positions and a significant computational time and memory required decrease.

1 INTRODUCTION

In the field of material sciences and structural analysis, micro-mechanical computational analysis has been widely utilized over the past few decades. Numerous techniques have been developed to simulate and predict properties and phenomena in various classes of materials, from metals to polymers to ceramics to composite materials [1]. The study of predicting mechanical properties, damage evolution and failure in heterogeneous materials like composite materials with continuous fibers has been an ever-growing area of research that more and more use the tools of micromechanical analysis to correctly understand the complex physical behavior that appears when combining different phases in uniform or non-uniform distributions (Figure 1).

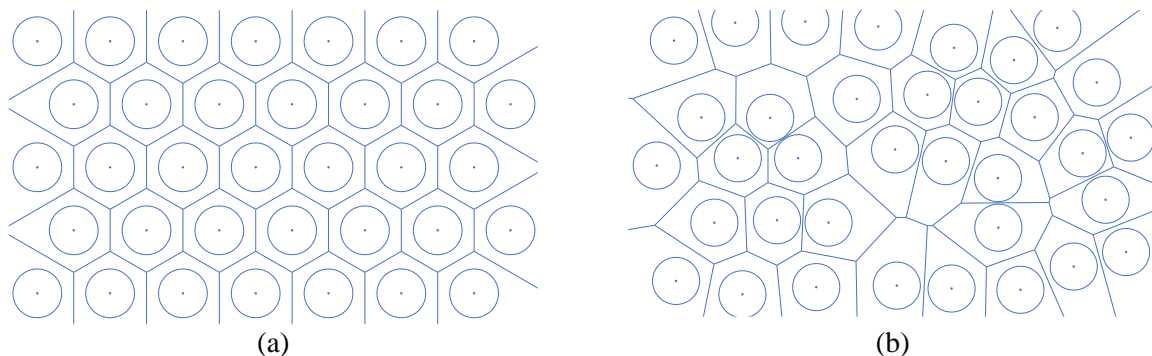


Figure 1: Composite microstructures with Voronoi cells for (a) uniform fiber distribution (b) non-uniform fiber distributions

To better understand the physical behavior of non-uniformly distributed fibers in composite materials manufactured out of continuous fibers, it is usual to use the Finite Element Method (FEM) to

create Representative Volume Elements (RVEs) containing hundreds of fibers and hundreds of thousands of elements to correctly predict the stress fields under different boundary conditions, which is a computationally expensive approach to both create the random distribution of fibers, and run the problem, especially when factoring number of degrees of freedom, memory allocation and size of the result files.

Instead, Voronoi tessellation can be employed; this approach considers the fibers' cross sections as perfect circles and represents the material as a collection of neighboring polygons with varying numbers of sides, each associated with a fiber center and its corresponding Voronoi cell [2]. This procedure creates a natural mesh for a composite microstructure, which helps the discretization of such problems to use in a finite element or generalized finite element approach, where each Voronoi cell can be considered the domain of a polygonal n -gon generalized element (Figure 1).

The concept of polygonal finite elements was first introduced by Ghosh in a series of works [3, 4, 5], and has the advantages of being able to create adaptive meshes that can better accommodate for complex geometries, especially when using randomly populated nodes inside bidimensional domains, but its applicability was limited at the time due to the available computational tools. Despite the advantages offered by polygonal finite elements, triangular and quadrilateral elements are generally preferred over polygons; several reasons contribute to this preference: the difficulty in creating a polygonal mesh, the challenge of finding a family of functions that cover the entire polygonal domain while maintaining the partition of unity property and sufficiently describes the boundaries, the complexity of both transforming n -gons to and from a parametric uniform domain and integrating over the domain. However, as previously discussed, the natural formation of polygonal meshes with different-sided polygons through Voronoi tessellation in composite micro-structures may prove advantageous if a way to incorporate the fibers or can be found.

Numerous studies have explored the use of polygonal finite elements. For example, [6] employed non-structured meshes with polygonal finite elements to accurately solve elastic problems such as cantilever beams and stress intensity factor calculations on crack edges. They used an integration strategy that divided the n -gon into n triangles using the barycenter and applied classic Gauss-Legendre quadrature to integrate over these triangular sub-domains. [7] implemented a Reissner-Mindlin polygonal membrane element with various families of barycentric shape functions (Wachspress, mean-value, Laplace, and piece-wise linear) and compared the solutions. [8] developed a high-order polygonal element integrated into a classic finite element method to study elasticity problems, including a unit cell for fiber-reinforced elastomer materials, which is relevant to the present work.

The Generalized Finite Element Method (GFEM), initially proposed by [9, 10, 11], extends the classic FEM shape functions by incorporating additional enrichment functions, either implicitly or explicitly, to better represent the behavior of the element domain under different circumstances. The goal of this approach is to enable the simulation of non-uniform composite microstructures using polygonal finite elements, with negligible computational cost, in regions where the full influence of fiber presence is not significant.

The present study showcases a novel approach for simulating non-uniform distributed fiber RVEs using a generalized finite element method. In this methodology, a Voronoi cell of a composite microstructure is treated as a single generalized element, where enrichment functions are employed to consider the stress effects of the fiber and the variation in elastic properties within its domain. The proposed method involves enriching a polygonal generalized finite element with a naturally occurring circular fiber within its domain. By using this approach together with leveraging the Voronoi tessellation of a microstructure and taking its cells as elements of a naturally occurring mesh, the simulation of composite microstructures becomes highly efficient. However, some problems exist with the approach such as the discretization of the boundary of the elements, the integration over the different domain, capturing the stress concentrations that naturally occur around the edges of the fiber, and the compatibility between the boundary of two neighboring elements. All these issues are solved using specially chosen enrichment functions and classic numerical techniques such as Lagrange penalization.

Although this approach does not strive for perfect accuracy when compared to traditional methods, its primary objective is to provide a computationally efficient procedure for simulating non-uniform

fiber unidirectional composite microstructures. The resulting simulations can be utilized in various applications, such as identifying critical regions through statistical analysis that require multiple realizations [12]. Additionally, they can be employed to generate synthetic populations for optimization purposes or for training artificial neural networks that study RVEs [13]. As such, by offering an efficient alternative to traditional methods, this generalized finite element approach opens new possibilities for advanced microstructure analysis and modeling.

2 MATHEMATICAL FORMULATION AND METHODOLOGY

The generalized polygonal finite element is a polygon of domain Ω that may be divided into two different domains containing the fiber and matrix phases Ω_f and Ω_m respectively such as $\Omega = \Omega_m \cup \Omega_f$; the boundary of this polygon Γ defined by n sides Γ_i such as $\Gamma = \cup_i \Gamma_i$ (n -gon –Figure 2). Follows a concise version of the formulation, based upon previous works of the author and other works [14, 15, 16].

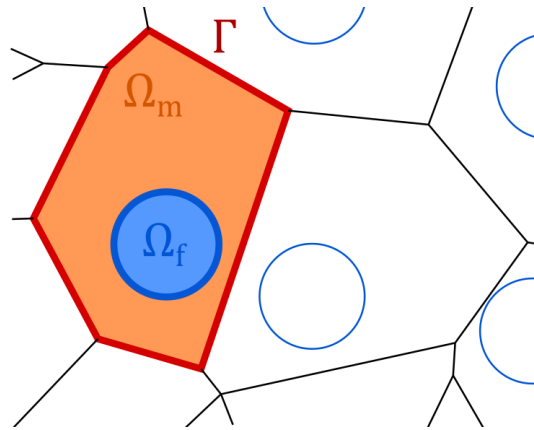


Figure 2: Domain nomenclature

2.1 Shape functions and enrichment functions

The proposed generalized finite element uses Wachspress functions [2] to establish the partition of unity base. These functions, denoted as φ_n , serve as fundamental shape functions basis for the element. Various methods exist for defining and computing Wachspress functions; in this formulation, we adopt an approach inspired by the work of [17], as presented in Equation 1. Here, the Wachspress functions φ_n are obtained by evaluating auxiliary area projection functions w , defined in Equation 2.

$$\varphi_n = \frac{w_n(P)}{\sum_k w_k(P)} \quad (1)$$

$$w_k = \frac{A(Q_{k-1}, Q_k, Q_{k+1})}{A(Q_{k-1}, Q_k, P)A(Q_k, Q_{k+1}, P)} \quad (2)$$

In this approach, the calculation of auxiliary functions for each point P inside a convex n -gon involves n distinct functions, each corresponding to a different vertex. To determine these auxiliary functions, the vertices of the n -gon are numbered in a counter-clockwise manner. For a given k -th vertex Q_k , the value of the corresponding k -th auxiliary area projection function w_k at point P is computed using three points: the preceding neighboring vertex Q_{k-1} , the current vertex Q_k , and the succeeding neighboring vertex Q_{k+1} . These auxiliary functions are defined as the ratio of the area formed by the three vertices (represented by the wavy region in Figure 3) to the product of the areas formed by the two projected triangles visible to point P (highlighted in blue and green in Figure 3). Implementation wise an explicit equation using the coordinates of P and the points Q_{k-1} , Q_k , and Q_{k+1} is used.

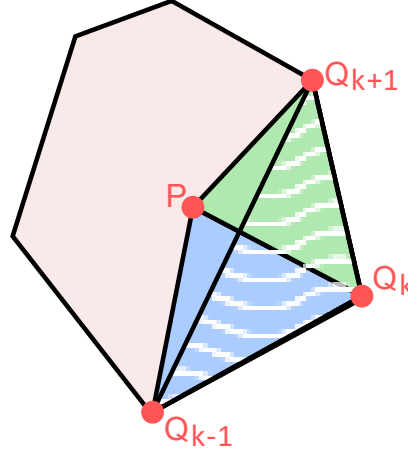


Figure 3: Area definitions for the calculation of the Wachspress functions

It should be noted that this definition is not valid when point P lies on one of the boundaries of the n -gon. In such cases, an approximation is employed by selecting a point P^* within a tolerance radius of P that lies inside the n -gon. The tolerance value should be chosen as small as possible and, through numerical experimentation, it was determined that the stability of calculations remained intact for tolerances as small as 10^{-16} ; this approach is of extreme importance for the integration of the generalized element over the domain $\Omega_m = \Omega \setminus \Omega_{\text{fiber}}$, since it imposes that quadrature rules used need to have strictly internal integration points.

The fundamental shape functions are then enriched by using locally defined enrichment functions as per the GFEM method. The enrichment functions work in two different groups: global enrichment functions ψ^g and stress concentration functions ψ^s .

The global enrichment functions serve to increase the degree of the discretization for low sided polygons like triangles or quadrilaterals, and to increase the degree of the discretization over the boundaries so that the strain distributions, and consequently the stresses, are not constant. This needs to be done so the strain compatibilization can be correctly evaluated between elements through a penalization procedure (See Session 2.2 and Equation 16). This is achieved by using a family of binomial polynomials written on the global x and y coordinates of the whole system, centered on the centroid of a given n -gon (\bar{x}, \bar{y}) . These functions can be written as.

$$\psi_{pq}^g(x, y) = (x - \bar{x})^p (y - \bar{y})^{q-p}, \quad p = 1..q \quad (3)$$

[18] created a method to procedurally develop high order Wachspress bases for any m -face polygon, and applied that to a Discontinuous Galerkin Method obtaining results similar to what is done on the present paper using the global enrichment functions .

The stress concentration enrichment functions ψ_s , are local to the element coordinates and work by using radial basis functions centered on the edge of the fiber to capture the stress concentration around the fiber. In particular, the approach taken in this paper is that n of such functions, each one centered on the intersection of the fiber edge to the line connecting two neighboring fibers. While this does not necessarily indicate a stress concentration region, most of the stress concentration points happens in areas close to these regions, and for the regions where that do not happen, the equilibrium will make it so the enriched degrees of freedoms will be small, coupled with the multiplying Wachspress functions this will suppress these regions and get the correct behavior.

Mathematically these can be written as, as per Figure 4.

$$\psi_p^s(x, y) = \begin{cases} e^{-\frac{(r-r_0)^2}{\sigma^2}}, & \text{if } (x, y) \in \Omega_m \\ 0, & \text{if } (x, y) \in \Omega_f \end{cases} \quad (4)$$

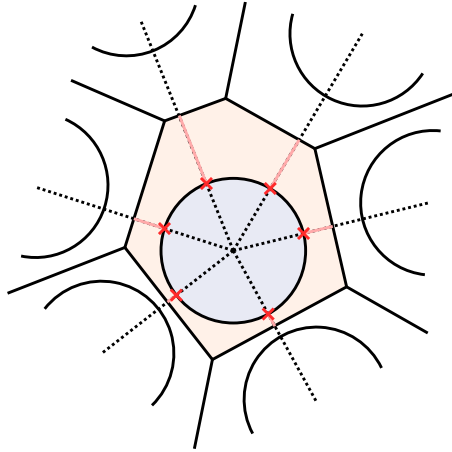


Figure 4: Geometric definitions for the stress concentration enrichment functions

As such the final shape functions of the element ϕ are written as:

$$\phi(x, y) = \varphi(\xi, \eta) + \varphi(\xi, \eta)\psi^g(x, y) + \varphi(\xi, \eta)\psi^s(x, y) \quad (5)$$

$$\phi = \varphi \otimes \{1 \quad \psi^g \quad \psi^s\} \quad (6)$$

where \otimes denotes the Kronecker product.

2.2 Element compatibility

Since neighboring elements may not necessarily have the same shape functions since these depend on both the number of sides of a particular Voronoi cells and the position of the fiber center in that element in relation to the boundaries, which may affect the stress concentration enrichment functions, the classical superposition method used for classic finite element method cannot guarantee a smooth transition of displacements and strains through the sides of each neighboring polygonal element.

The compatibility between neighboring elements is therefore imposed through a penalization condition using Lagrange multipliers on every common side Γ ; in Equation 7 this is identified as Γ^- and Γ^+ for two neighboring elements, where the minus indicates the element with the smaller numbering identification in an algorithmic implementation. Equation 7 therefore describes the extra terms of virtual energy created in the system by the compatibility occurring in the common side Γ

$$\delta\Pi_\Gamma = \delta(\oint_\Gamma \lambda_u \cdot (u|_{\Gamma^-} - u|_{\Gamma^+})d\Gamma) \quad (7)$$

This penalization is continuous through every Γ_i side using classic unidimensional cubic Hermite polynomials χ for the discretization of the penalizing forces λ , found in Equations 8 and 9, where the ζ coordinate is a local coordinate existing in the Γ_i side, varying from $[-1, +1]$, as per Figure 5.

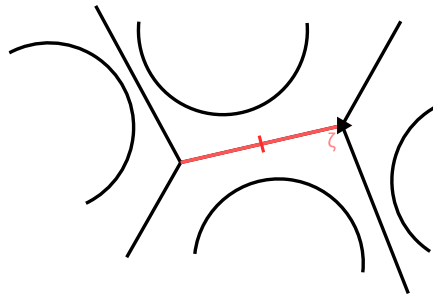


Figure 5: Local boundary coordinate definition

$$\chi = \begin{cases} \frac{1}{2}(1 - \zeta) - \frac{1}{2}(1 - \zeta^2) + \frac{1}{16}(-9\zeta^3 + \zeta^2 + 9\zeta - 1) \\ \frac{1}{2}(1 + \zeta) - \frac{1}{2}(1 - \zeta^2) + \frac{1}{16}(+9\zeta^3 + \zeta^2 - 9\zeta - 1) \\ (1 - \zeta^2) + \frac{1}{16}(27\zeta^3 + 7\zeta^2 - 27\zeta - 7) \\ \frac{1}{16}(-27\zeta^3 - 9\zeta^2 + 27\zeta + 9) \end{cases} \quad (8)$$

$$\lambda = \xi_p \lambda_p \quad (9)$$

2.3 Governing equations and numerical integration

An isoparametric space is needed to define the integration points of the quadrature. By utilizing the Wachspress functions φ_n , the polygonal finite element can be mapped to an isoparametric space, where the n -gon is inscribed within a unit circle, as depicted in Figure 6 for a pentagonal unit cell. Figure 6 also illustrates the impact of the isoparametric transformation on the fiber. A perfectly circular fiber undergoes distortion, and its boundaries are not trivially identifiable. In this work, the boundary is determined by inverting the isoparametric relation using a Newton-Raphson procedure.

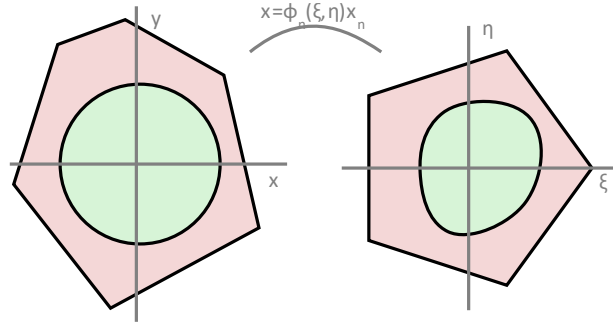


Figure 6: Transformation from parametric and global system

The final elemental energetic contributions to the equilibrium equation Π_{elem} is written as:

$$\begin{aligned} \delta \Pi_{elem} = & \delta u^T \left(\int_{\Omega} B^T C_m B d\Omega + \int_{\Omega_f} B^T (C_f - C_m) B d\Omega \right) u + \delta u^T \left(\oint_{\Gamma} (N_{\phi}^-|_{\Gamma^-} - N_{\phi}^+|_{\Gamma^+})^T N_{\lambda} d\Gamma \right) \lambda + \\ & \delta \lambda^T \left(\oint_{\Gamma} N_{\lambda}^T (N_{\phi}^-|_{\Gamma^-} - N_{\phi}^+|_{\Gamma^+}) d\Gamma \right) u - \delta u^T \left(\int_{\Omega} N_{\phi} b d\Omega + \oint_{\Gamma_f} N_{\phi} |_{\Gamma_f} t d\Gamma_f \right) \end{aligned} \quad (10)$$

where N_{λ} , N_{ϕ} , B are the classic displacement and strain discretization matrixes but using the enriched shape functions, and C_f and C_m are the classic plane strain constitutive matrices.

$$N_{\lambda} = \begin{bmatrix} \chi \otimes \{1 & 0\} \\ \chi \otimes \{0 & 1\} \end{bmatrix} \quad (11)$$

$$N_{\phi} = \begin{bmatrix} \phi \otimes \{1 & 0\} \\ \phi \otimes \{0 & 1\} \end{bmatrix} \quad (12)$$

$$B = \begin{bmatrix} \phi_{,x} \otimes \{1 & 0\} \\ \phi_{,y} \otimes \{0 & 1\} \\ \phi_{,x} \otimes \{0 & 1\} + \phi_{,y} \otimes \{1 & 0\} \end{bmatrix} \quad (13)$$

$$C_{m|f} = \frac{E_{m|f}}{(1+\nu)(1-2\nu)} \begin{bmatrix} 1 - \nu_{m|f} & \nu_{m|f} & 0 \\ \nu_{m|f} & 1 - \nu_{m|f} & 0 \\ 0 & 0 & \frac{1-2\nu_{m|f}}{2} \end{bmatrix} \quad (14)$$

Which can be summarized in matrix form as:

$$\begin{bmatrix} K & L^T \\ L & \underline{0} \end{bmatrix} \begin{Bmatrix} u \\ \lambda \end{Bmatrix} = \begin{Bmatrix} F \\ \underline{0} \end{Bmatrix} \quad (15)$$

Where K is a matrix containing every local stiffness matrix of every n -gon element without superposition, relating to duplicate degrees of freedom in neighboring elements, F is a force vector integrated over the either the whole system for body efforts b or over defined boundary conditions Γ_f with traction efforts t and L is a matrix containing a set of penalization equation through every side created in the Voronoi diagram shared by two cells, each pair generating a matrix L_Γ for that side Γ . Though concentrated efforts could be accounted for energy wise in the formulation, they are neglected in the present formulation due to not naturally occurring in the equilibrium and possibility creating singularities with the penalizations and the enrichments.

To account for the different elastic properties existing between the two different phases, the integration of the elemental stiffness matrixes K_{elem} is made through the summation of the Ω_m domain with the matrix constitutive matrix C_m and the Ω_f domain with “fiber minus matrix” constitutive matrix $C_f - C_m$.

$$K_{elem} = \int_{\Omega} B^T C_m B d\Omega + \int_{\Omega_f} B^T (C_f - C_m) B d\Omega \quad (16)$$

$$L_\Gamma = \oint_\Gamma N_\lambda^T (N_\phi^-|_{\Gamma^-} - N_\phi^+|_{\Gamma^+}) d\Gamma \quad (17)$$

The integration of stiffness matrix is done in a simple way by separating the n -gon into n triangles and the circle domain (Figure 7). Each triangle is integrated using an adaptative Xiao-Gimbutas [19]. This particular quadrature was chosen for having strictly internal integration points, which could create problems if it was not the case for how the Wachspress functions were defined on the boundary. The circle domain is then integrated using a King-Song adaptative quadrature [20], which does not suffer from the same problem; in fact, some outside points were found to be in fact desirable with this approach since that contributes to affect the stress concentration enrichment function on the fiber domain. Adaptative quadrature were chosen since the degree of the Wachspress functions and the global enrichment functions varies depending on the number of sides of each polygonal element, and as such, a single degree of integration cannot guarantee an exact result for every possible domain.

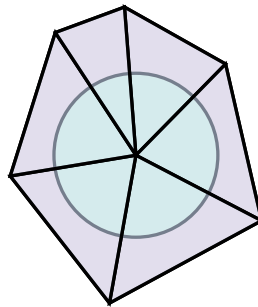


Figure 7: Integration domains

3 NUMERICAL CASE STUDIES

Several different case studies were conducted by first analyzing composite microstructures with different volume fractions ($v = 40.75\%, 61.90\%, 69.87\%$) [21] and obtaining Weibull statistical distributions that generate their non-uniform fiber distributions.

For the present work, the images were analyzed by initially developing a code that identifies the radius and positions of fibers within the material sample through algorithms based on Laplacians of color layers of expanded matrices from image files (Figure 8).

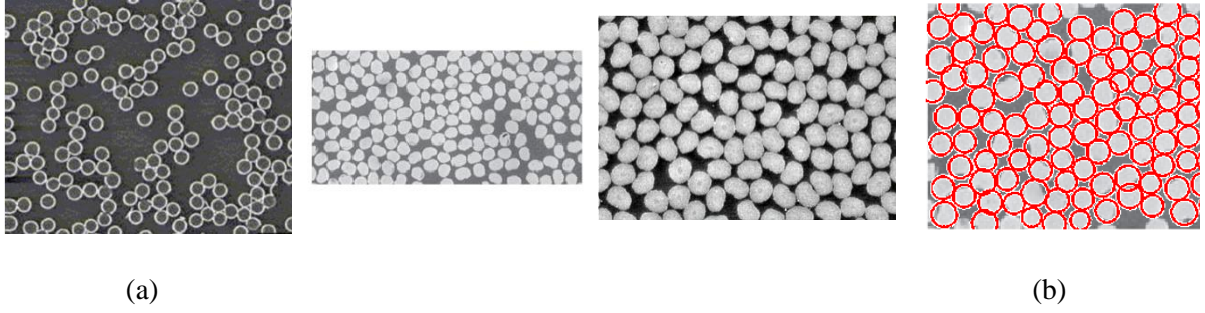


Figure 8: (a,b,c) Example of microscopy or SEM original images [21], (d) Fiber identification algorithm

The distribution of fiber center positions is then adjusted to a hexagonal uniform distribution created with a fiber volume fraction equivalent to the original image material, using a genetic optimization algorithm. The obtained quantities are adjusted to a Weibull-type statistical distribution using the maximum likelihood analysis relationships contained in Equations 11 and 12 [22].

$$k_{j+1}^{-1} = \frac{\sum_{i=1}^n x_i^{k_j} \ln x_i}{\sum_{i=1}^n x_i^{k_j}} - \frac{1}{n} \sum_{i=1}^n x_i^{k_j} \ln x_i \quad (11)$$

$$\lambda_j = \frac{1}{n} \sum_{i=1}^n x_i^{k_j} \quad (12)$$

Based on these parameters, possible uniform or non-uniform fiber distribution models can be created, as well as finite element models. Examples of this procedure and possible realizations are shown in Fig. 9 below.

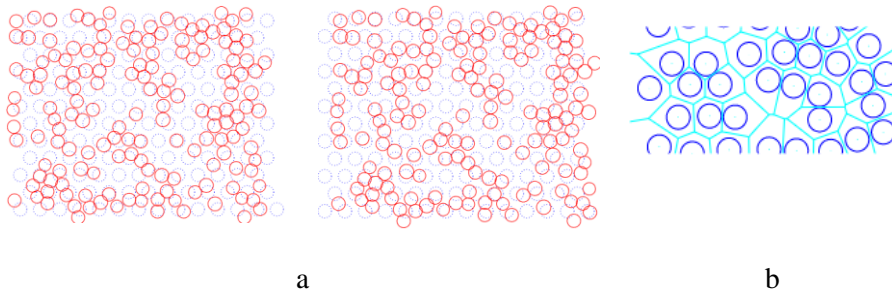


Figure 9: (a) Optimization procedure, (b) Obtained realization of the non-uniform distribution

Three realizations, one for each of those material cases were chosen, an example of which for the first case can be seen on Figure 10. These realizations define an RVE with approximately 20 x 10 fibers, some near the edges which were suppressed, and were simulated using the present work element and ABAQUS commercial finite element software for simple traction and shearing boundary conditions, as per the diagrams in Figure 11.

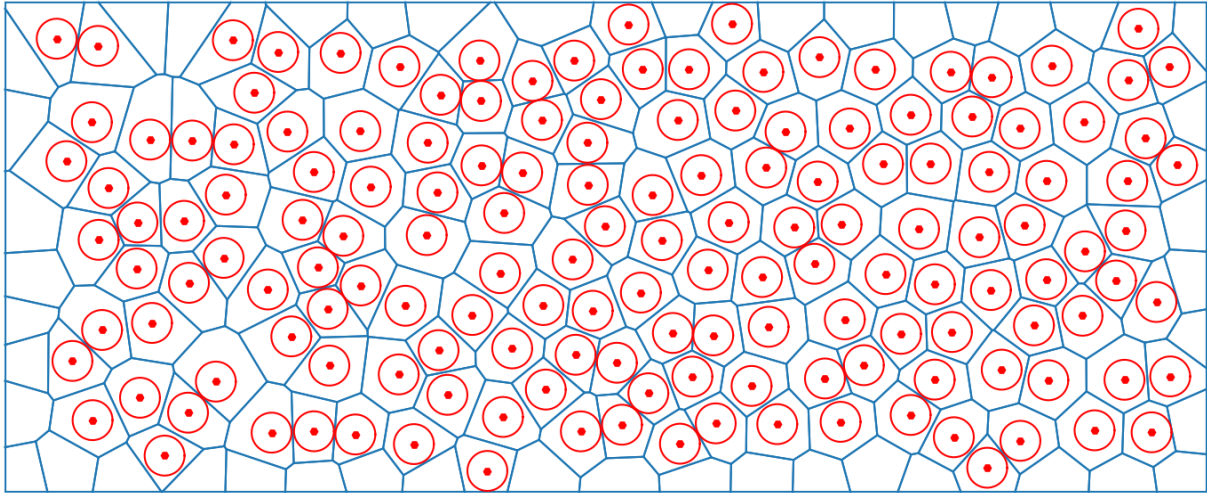


Figure 10: Example of realization used for the study cases

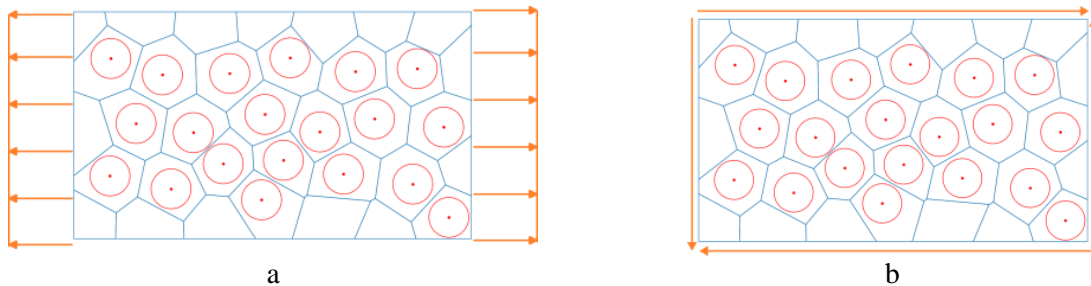


Figure 11: (a) Traction boundary conditions, (b) Shear boundary conditions

Even though the images from each reference are manufactured with different matrices and fibers, for numerical verification of the model all cases are run with the same material properties, typical properties for carbon fiber and epoxy matrix, found in Table 1 below.

Table 1: Properties for simulations

E_f [GPa]	ν_f []	E_m [GPa]	ν_m []
127	0.324	8.93	0.224

The number of degrees of freedom on each model and the relative difference for displacements, maximum stress values and position of these maximum stress were compared between the two, as well as the computational time it took.

4 RESULTS

Three realizations for each of the volume fractions described in the previous section were simulated using both the present model and ABAQUS. Table 2 contains the average number of number of degrees of freedom obtained for convergence and the computational time needed to solve the system for each load case using a simple laptop for the three cases. Table 3 shows the maximum displacement for each of the cases and the difference obtained between the current work and ABAQUS.

Table 2: Degrees of freedom and computational times

Volume fraction of fiber [%]	Solver	Number of degrees of freedom for convergence	Time [s]
40.75	Present Work	4423	7.636
	ABAQUS	5930564	1273.2
61.90	Present Work	4940	8.536
	ABAQUS	6349848	1402.3
68.87	Present Work	4780	7.838
	ABAQUS	6018381	1313.5

Table 3: Results for different study cases

Volume fraction of fiber [%]	Load case	Solver	Maximum normalized displacement	Average principal stress	Maximum principal stress
40.75	Traction	Present Work	0,1034	14,0260	519,3400
		Abaqus	0,1034	14,0260	451,8258
	Shear	Present Work	0,1450	19,6690	728,2814
		Abaqus	0,1450	19,2756	633,6048
61.90	Traction	Present Work	0,0887	12,0320	445,5073
		Abaqus	0,0888	11,8962	386,6903
	Shear	Present Work	0,1043	14,1481	523,8604
		Abaqus	0,1043	13,8181	437,9473
68.87	Traction	Present Work	0,0768	10,4178	385,7380
		Abaqus	0,0768	10,2995	356,0362
	Shear	Present Work	0,0993	13,4698	498,7472
		Abaqus	0,0992	13,4240	459,8801

It can be seen from both tables that the number of degrees of freedom was about three orders of magnitude lower than the ones needed in the classic method to obtain convergence of maximum stress values. When separating the total time spent on Abaqus solution, the more than 68% of the time was taken by mesh generation (for example, in the first case it took 123 s on geometry creation, 873 s on mesh generation and 240 s on system solution), showing the main advantage of the method. The accuracy of maximum displacements was deemed to be good of 99% but given these are primary variables of the weak problem this is to be expected. The values of average stresses were found to be accurate which were deemed to be acceptable given the increased computational efficiency obtained. The values of maximum stresses were not as coherent which makes sense since the enrichment functions do not perfectly capture the physical behavior of clustering of fibers.

However, when looking at the position of the largest stresses values the present methodology can correctly predict the location of stress concentration, which is a good result for the creation of synthetic populations for training of neural networks that may analyze UD composite microstructures.

5 CONCLUSIONS

The results obtained with the present methodology and a classical approach using a commercial solution with ABAQUS were compared: the accuracy in displacements, which for benchmarks tested was over 98%, accuracy in strains, which for benchmarks tested was an average of over 90%, computational time, and number of degrees of freedom and were both reduced by three orders of magnitude. The last result is a particular interesting result for use within optimization and artificial neural networks.

ACKNOWLEDGEMENTS

The author would like to thank Financiadora de Estudos e Projetos (FINEP) for partially funding the work through the grant MCTIC/FINEP/CT-INFRA Campi universitários regionais e novas universidades 02/2018; Referência: 0527/18.

REFERENCES

- [1] R. Talreja, Modeling damage, fatigue and failure of composite materials, Cambridge, UK: Woodhead Pub, 2016.
- [2] N. Sukumar and E. A. Malsch, "Recent advances in the construction of polygonal finite element interpolants," *Archives of Computational Methods in Engineering*, vol. 13, p. 129–163, March 2006.
- [3] S. Ghosh and R. L. Mallett, "Voronoi cell finite elements," *Computers & Structures*, vol. 50, p. 33–46, March 1994.
- [4] S. Ghosh, K. Lee and S. Moorthy, "Multiple scale analysis of heterogeneous elastic structures using homogenization theory and voronoi cell finite element method," *International Journal of Solids and Structures*, vol. 32, p. 27–62, January 1995.
- [5] S. Ghosh, K. Lee and S. Moorthy, "Two scale analysis of heterogeneous elastic-plastic materials with asymptotic homogenization and Voronoi cell finite element model," *Computer Methods in Applied Mechanics and Engineering*, vol. 132, p. 63–116, May 1996.
- [6] A. Tabarraei and N. Sukumar, "Application of polygonal finite elements in linear elasticity," *International Journal of Computational Methods*, vol. 03, p. 503–520, December 2006.
- [7] H. Nguyen-Xuan, "A polygonal finite element method for plate analysis," *Computers & Structures*, vol. 188, p. 45–62, August 2017.
- [8] H. Chi, C. Talischi, O. Lopez-Pamies and G. H. Paulino, "A paradigm for higher-order polygonal elements in finite elasticity using a gradient correction scheme," *Computer Methods in Applied Mechanics and Engineering*, vol. 306, p. 216–251, July 2016.
- [9] J. M. Melenk, On Generalized Finite Element Methods, University of Maryland at College Park, 1995.
- [10] T. Strouboulis, I. Babuška and K. Copps, "The design and analysis of the Generalized Finite Element Method," *Computer Methods in Applied Mechanics and Engineering*, vol. 181, p. 43–69, January 2000.
- [11] T. Strouboulis, K. Copps and I. Babuska, "The generalized finite element method: an example of its implementation and illustration of its performance," *International Journal for Numerical Methods in Engineering*, vol. 47, p. 1401–1417, March 2000.
- [12] S. A. Elnekhaily and R. Talreja, "Effect of axial shear and transverse tension on early failure events in unidirectional polymer matrix composites," *Composites Part A: Applied Science and Manufacturing*, vol. 119, pp. 275-282, 2019.
- [13] Z. Yang, C.-H. Yu, K. Guo and M. J. Buehler, "End-to-end deep learning method to predict complete strain and stress tensors for complex hierarchical composite microstructures," *Journal of the Mechanics and Physics of Solids*, vol. 154, p. 104506, 2021.
- [14] M. Sartorato, "A numerical homogenization technique for unidirectional composites using polygonal generalized finite elements," *Proceedings of the Institution of Mechanical Engineers, Part L: Journal of Materials: Design and Applications*, vol. 236, pp. 1351-1363, 2022.
- [15] S. Ghosh, Micromechanical analysis and multi-scale modeling using the Voronoi cell finite element method, Boca, Raton: CRC Press, 2009.
- [16] S. Ghosh, Micromechanical Analysis and Multi-Scale Modeling Using the Voronoi Cell Finite Element Method, CRC Press, 2011.
- [17] M. S. Floater, K. Hormann and G. Kós, "A general construction of barycentric coordinates over

- convex polygons," *Advances in Computational Mathematics*, vol. 24, p. 311–331, January 2006.
- [18] D. Labeurthre, A. Calloo and R. Le Tellier, "High-order Wachspress functions on convex polygons through computer algebra," *J. Comput. Phys.*, vol. 470, p. 111545, December 2022.
- [19] H. Xiao and Z. Gimbutas, "A numerical algorithm for the construction of efficient quadrature rules in two and higher dimensions," *Comput. Math. Appl.*, vol. 59, p. 663–676, January 2010.
- [20] K. Kim and M. Song, "Symmetric quadrature formulas over a unit disk," *Han-gug Jeonsan Suhag Hoeji*, vol. 4, p. 179–192, March 1997.
- [21] V. Srinivasa, V. Shivakumar, V. Nayaka, S. Jagadeeshaiih, M. Seethram, R. Shenoy and A. Nafidi, "Fracture morphology of carbon fiber reinforced plastic composite laminates," *Materials Research*, vol. 13, p. 417–424, September 2010.
- [22] A. Papoulis, *Probability, random variables, and stochastic processes*, McGraw-Hill, 2002, p. 852.